Lack of cortistatin worsens neurological outcome and exacerbates aging-related glial and vascular dysfunction in stroke

Castillo-González J[1*], Vargas-Rodríguez P[1], Serrano-Martínez I[1], Forte-Lago I[1], Price M[2,3], Buscemi L[2,3], Hirt L[2,3], González-Rey E[1*].

[1]Institute of Parasitology and Biomedicine (IPBLN-CSIC), Granada, Spain; [2]University of Lausanne, Lausanne, Switzerland; [3]Lausanne University Hospital, Lausanne, Switzerland; [4]Medicine School, University of Granada, Granada, Spain

*Correspondence: elena.g@csic.es; juliacastillo@ipb.csic.es; Tel.: +34-958-181670

Summary

Ischemic stroke is the second leading cause of death globally. Neuroinflammation, blood-brain barrier (BBB) disruption, and immune dysregulation are key features of the pathogenesis and clinical outcomes of brain ischemia. A comprehensive understanding of the interconnected mechanisms and endogenous mediators that regulate these processes is essential for the development of effective therapeutic strategies. In this context, the present study investigates the role of cortistatin, a neuropeptide broadly distributed within the central nervous and immune systems. Given its anti-inflammatory, immunomodulatory, and neuroprotective properties, cortistatin positions as a promising endogenous factor in the pathogenesis of ischemic stroke. To evaluate its potential effects, we employed the widely recognized preclinical model of stroke, middle cerebral artery occlusion (MCAO), in young (3 months) and middle-aged (6 months) cortistatin-deficient mice and compared them with wild-type mice, assessing both short-term (48 hours) and long-term (7 days) outcomes. Our findings indicate that cortistatin deficiency in both young and middle-aged mice results in increased susceptibility to stroke and a significantly worsened prognosis, characterized by severe neurological deficits, altered microglial activity, impaired astrocytic scar formation, BBB disruption, dysregulated angiogenesis, and exacerbated immune infiltration and peripheral immune responses. Notably, the administration of cortistatin reversed these adverse outcomes, underscoring the critical role of cortistatin in regulating the complex interactions between the nervous and immune systems. Furthermore, cortistatin treatment for one week markedly improved key processes involved in stroke recovery, including neuronal repopulation, myelin repair, and the restoration of BBB integrity. The multifaceted therapeutic effects of cortistatin across various pathological stages and phenotypes suggest that multimodal therapies could represent a novel and more effective approach for treating ischemic stroke, offering advantages over current interventions that typically target only a single aspect of stroke pathology. In conclusion, our findings emphasize the significance of identifying the endogenous and therapeutic roles of neuro-immune mediators such as cortistatin in ischemic stroke.

INTRODUCTION

Ischemic stroke is the second leading cause of death worldwide and the main cause of disability in adults [1]. The blockage of cerebral blood flow due to the occlusion of a brain artery, followed by reperfusion, triggers a complex cascade of intricately interconnected events. Neuroinflammation,

blood-brain barrier (BBB) breakdown, and immune deregulation are the major hallmarks of the pathogenesis and outcomes of brain ischemia [2]. Despite improvements in recanalization treatments, current therapeutic options remain limited to intravenous rtPA or endovascular thrombectomy, both of which have a narrow therapeutic window and carry significant side effects [3]. Therapeutic shortcomings primarily arise from the simplistic use of preclinical animal models (*i.e.,* excluding risk factors such as aging or hypertension), administration of drugs with a single spectrum of action in a multifactorial process, and reliance on immunosuppressants rather than immunomodulators. Additionally, the complex and not yet fully understood spatiotemporal pathophysiology of stroke presents further challenges [4], as it involves numerous simultaneous cellular and molecular mechanisms affecting the brain, vascular system, and peripheral organs, many of which are often overlooked. Therefore, there is an urgent need to fully understand the neuro-immunological context and the endogenous factors involved at the different stages and contexts of ischemic pathology (*i.e.,* short- and long-term outcomes) to develop more effective therapeutic strategies.

The neuropeptide cortistatin is widely distributed, alongside its receptors, in both the central nervous system (CNS) and the immune system [5,6]. Although it shares significant homology, functions, and receptors (Sst1-5) with somatostatin, cortistatin plays distinct roles in the nervous system and peripheral tissues [7,8], thanks to its ability to bind to additional receptors, including the ghrelin receptor (Ghsr), the Mas gene-related receptor X-2 (MrgX2), and a yet unidentified cortistatin receptor. Remarkably, cortistatin exhibits potent immunomodulatory, anti-inflammatory, and neuroprotective effects in models of neuroinflammatory and neuroimmune disorders, such as multiple sclerosis [9], excitotoxicity [10], meningoencephalitis [11], neuropathic pain [12], or Parkinson's disease [13]. In these models, cortistatin reduces inflammatory mediators, regulates glial cell function, and maintains tissue-surveillance activities, protecting against disease development and progression. Cortistatin also plays a crucial role in maintaining BBB integrity and function by regulating tight-junctions proteins and exerting anti-inflammatory effects in endothelial cells, thereby protecting against ischemic damage and barrier leakage [14]. Remarkably, recent studies from our group have unveiled the potential therapeutic role of cortistatin in ischemic stroke when administered 24 h post-stroke in young mice, modulating glial reactivity and astrocytic scar formation, facilitating BBB recovery, and regulating local and systemic immune dysfunction [15]. However, the long-term effects of cortistatin treatment and its importance in stroke-associated risk factors remain unexplored. Similarly, the endogenous role of this neuropeptide in ischemic stroke pathophysiology has yet to be fully understood. In this context, previous studies from our group have demonstrated that the absence of cortistatin is linked to an exacerbated pro-inflammatory basal state in the CNS and periphery, and reduced expression of neurotrophic factors [6,9]. Additionally, previous results have described exacerbated inflammatory responses in cortistatin-deficient mice [9], worsened outcomes in models of inflammation or neuronal damage [9,12,16], and the manifestation of a premature aging phenotype (preliminary data of the group).

Given the important roles demonstrated by cortistatin in neuroprotection, immunomodulation, anti-inflammatory responses, and BBB protection in neurodegenerative and neuroimmune disorders, along with its therapeutic effects in ischemic stroke when administered at 24 h, we aim to further evaluate the endogenous function of this neuropeptide. Specifically, this study will examine for the first time the role of cortistatin in neuronal damage, neurological outcomes, glial responses, vascular and barrier changes, and peripheral immune activation in young and middle-aged cortistatin-deficient mice, focusing on both short- and long-term outcomes, to provide a comprehensive understanding of the spatiotemporal dynamics of stroke. Additionally, the therapeutic potential of cortistatin in restoring the ischemic stroke phenotype will be evaluated under these conditions.

MATERIALS AND METHODS

Peptides

Mouse CST-29 was obtained from Bachem and dissolved in distilled water to a final concentration of 10^{-4} M from its lyophilized form.

Animals

The procedures outlined in this study were approved by the Animal Care and Use Board and the Ethical Committee of the Spanish National Research Council (Animal Care Unit Committee IPBLN-CSIC # protocol CEEA OCT/2017.EGR), and conducted in accordance with Directive 2010/63/EU of the European Parliament on the protection of animals used for scientific purposes. Transgenic mice lacking the cortistatin gene (*Cort*$^{-/-}$) were a generous gift of Dr Luis de Lecea (Stanford University, United States) generated and maintained within a C57BL/6J background, following the methods previously described [7]. Mice were housed in groups of ten per cage in a controlled environment (22 ± 1ºC, 60-70 % relative humidity), and subjected to a 12 h light/dark cycle (lights on at 7:00 a.m.), and had *ad libitum* access to food and water.

Transient middle cerebral artery occlusion model

Young (12 weeks old) and middle-aged (6 months old) *Cort*$^{+/+}$ and *Cort*$^{-/-}$ mice were subjected to MCAO model [17]. Mice were anesthetized under isoflurane (1.5-2 % in 70 % N_2O / 30 % O_2) using a facemask and administered meloxicam (2 mg/kg, subcutaneously, Norbrook) for post-surgery analgesia. Body temperature was maintained constant throughout the surgery using a heating pad. The regional CBF (rCBF) was monitored by laser Doppler flowmetry (moorVMS-LDF1, Moor Instruments) fixing a probe on the skull over the core area supplied by the MCA (approximately 1 mm posterior and 6 mm lateral from the bregma). Transient focal ischemia was induced by introducing a silicon-coated filament (701756PK5Re, Doccol) through the left common carotid artery into the internal carotid artery until reaching and occluding the middle cerebral artery. The filament was placed here for 20/35 minutes for young and middle-aged mice respectively. After this time the filament was withdrawn to allow reperfusion. Surgery was considered successful when the flow dropped down to < 20 % of the baseline during the occlusion, and when it reached > 50 % of the

baseline after reperfusion. Mice were housed in their cage until sacrifice, with *ad libitum* access to food and water. Each cage was equipped with water-softened chow and recovery gel.

Cortistatin (1 nmol in PBS) was intraperitoneally administered 24 h after MCAO once (48 h) or daily (7 days). Controls were injected with the same amount of saline solution. Neurological score, behavioural tests, ischemic volume determination, morphometric characterization of glial populations, and inflammatory response, were determined 48 h and 7 days after surgery.

Neurological score

The functional outcome of each mouse was assessed by a neurological score evaluation each 24 h after MCAO and before sacrifice. Severity was graded from 0 to 3 evaluating motor, sensory, reflex, and balance using a compendium of previously published scales [18,19].

Ischemic lesion volume determination

48 h after MCAO surgery, mice were sacrificed by an overdose of intraperitoneal injection of ketamine (100 mg/kg, Ritcher Pharma) and xylazine (10 mg/kg, Fatro Iberica) and intracardially perfused with 4 % PFA. Brains were dissected and fixed in 4 % PFA for 24 h at 4 ºC and cryoprotected in 30 % sucrose for 48 h at 4 ºC. Brains were then frozen in isopentane in dry ice at - 25 ºC and stored at - 80 ºC until use. Brains were cut into 20 µm coronal sections with a cryostat.

Cresyl violet-stained sections (gradual hydration in ethanol, stained with 1 mg/ml of CV-acetate in distilled water, gradually dehydrated in ethanol, and clear in xylene) [19] were imaged under a Leica DM2000 Transmit stereomicroscope at 2.5x magnification. The infarct volume was calculated by multiplying the sum of the infarcted areas on each section by the spacing distance using the ImageJ Fiji free software.

Immunofluorescence

For immunofluorescence labelling, 20 µm free-floating sections were washed with PBS and blocked and permeabilized with PBS 1x, 1 % BSA, 0.1 % Triton X-100, and 5 % goat serum for 60 min at RT. Then, sections were incubated with primary antibodies anti-MAP2 (1:1000, Sigma), anti-Iba1 (1:1000, Wako), anti-GFAP (1:5000, Dako), anti-CD31/PECAM-1 (1:300, BD), anti-ZO-1 (1:100, Fisher), or APC-labelled anti-CD45 (1:200, BD) in PBS 1x, 1 % BSA, 0.1 % Triton X-100, and 5 % goat-serum O/N at 4 ºC. Next, sections were washed with PBS and incubated with the corresponding secondary Alexa Fluor-conjugated antibodies (1:1000, Sigma) and DAPI in PBS 1x, 1 % BSA, 0.1 % Triton X-100, and 2 % goat-serum for 60 min. Sections were mounted with Mowiol. For IgG staining, the procedure remained the same, an Alexa Fluor 594-conjugated goat anti-mouse IgG antibody was utilized without a primary antibody. Images were taken with a LEICA DMi8 S Platform Life-cell microscope at 20x and with a confocal Leica TCS SP8 STED microscope at 63x.

Morphometric characterization

To thoroughly characterize the intricate and di and diverse morphology of microglia, and astrocytes after a stroke, we performed multiple morphometric analyses. First, individual microglia from specific brain regions (*i.e.,* periinfarct area for studying glial scar and microglia) were randomly selected. Careful attention was given to avoid cell overlap and to ensure that the entire nucleus and branches of each cell were captured. A total of 15-30 cells from each mouse (n = 15-30) across 3-6 mice (N = 3-6) were analysed. The images were processed using ImageJ Fiji software, following a systematic protocol adapted from previous studies [13,20,21]. First, the image was transformed to 8-bit grayscale and pre-processed to reduce background noise and enhance contrast. Second, images were binarized by applying a pre-established threshold. Next, extraneous pixels that did not correspond to cells were eliminated with the tools *Remove outliers* and *Despeckle*. In cases where the original image contained a significant amount of background noise, careful manual editing was performed.

After processing the images, the Skeleton and Fractal Analysis plugins of ImageJ Fiji software [22] were employed using the following parameters. For Skeleton Analysis, the number of junctions and maximum branch length were evaluated. For Fractal Analysis, span ratio (*i.e.,* the ratio of the axes of the convex hull from major to minor), convex hull area (*i.e.,* the area containing the entire cell shape enclosed by the smallest convex polygon), or fractal dimension (*i.e.,* index of complexity) were evaluated. See the user manual for more details.

Determination of the peripheral immune response

To evaluate the peripheral immune response, spleens were collected and weighed. The tissue was then gently ground on a 100 mm culture dish using the frosted edges of two slides. The homogenized tissue was transferred into RPMI medium supplemented with 10% FBS, 2 mM L-glutamine, 1% P/S, and 50 µM 2-mercaptoethanol. Then, the suspension was let to sit on ice for 5 min and the cell suspension was carefully collected and centrifuged at 1,670 rpm for 10 min at 4°C. The resulting pellet was resuspended in Ack buffer (150 mM NH4Cl, 10 mM KHCO3, 0.1 mM Na2EDTA) for 10 min at RT to lyse red blood cells. RPMI medium was then added, and the cells were centrifuged at 1,670 rpm for 10 min at RT before counting.

2.9. RNA extraction and evaluation of gene expression

After MCAO, brains were collected and separated into contralateral and ipsilateral sides in both control and cortistatin-treated mice. For RNA isolation, brain tissues were placed in TriPure reagent (Roche). Subsequently, cDNA synthesis was performed using the RevertAid First Strand cDNA Synthesis Kit (ThermoFisher) with random hexamers in a CFX Connect QPCR System (Biorad) under the following conditions: incubation at 25°C/5 min, reverse transcription at 42°C/60 min, inactivation at 70°C/5 min. Gene expression analysis was conducted using conventional qPCR. cDNA corresponding to 20ng of RNA was added to the SensiFast Sybr No-Rox kit 1x (Bioscience), along with the appropriate forward and reverse primers for each gene, and nuclease-free water to a

final volume of 20µl. The reaction was conducted in a CFX96 thermocycler (BioRad) under the following conditions: 94°C/5min (polymerase activation) followed by 40 cycles at 94°C/30s (denaturalization), 58°C/60°C/62°C/30 s (primer annealing temperature depending on the gene), and 72°C/30 s (extension). Quantification was performed using the comparative threshold cycle (Ct) method, with each gene's Ct values normalized to those of the housekeeping gene *Rplp0* within each PCR reaction. The fold change was calculated using the ΔΔCt method. The specific primers for each gene are listed in Additional File 1: Tables S1.

Statistical analysis

Data are expressed as the mean ± SEM. All experiments were randomized and blinded for researchers. The number of independent animals is shown (N) as well as the number of sections, cells, or structures analysed in each case (n). Statistical analysis was conducted using these independent values. Statistical differences comparing two groups were performed by using the unpaired Student's t test (for parametric data, and normal distribution) or the non-parametric Mann-Whitney U-test. For three or more groups with normal distribution and parametric data, one-way ANOVA with appropriate *post-hoc* tests for multiple comparisons was utilized (with a small number of data Bonferroni *post-hoc* test was preferentially used *vs* Tukey *post-hoc* test). Non-parametric data from three or more groups was analysed by Kruskal-Wallis test and Dunn *post-hoc* test. When standard deviations were assumed to be different, Brown-Forsythe and Welch ANOVA test were applied with Dunnett T3 *post-hoc* test. Spearman´s correlation non-parametric test was used for correlation studies. All analyses were performed using GraphPad Prism v8.3.0 software. We considered P-values < 0.05 (two-tailed) as significant.

RESULTS

Deficiency of cortistatin is linked to exacerbated neurodegeneration and impaired neuroinflammatory response which is modulated after cortistatin treatment

To investigate the endogenous role of the neuropeptide in ischemic stroke, we conducted the MCAO model, a well-established preclinical model that closely mimics the human ischemic condition [23]. MCAO procedure was conducted in young (3 months old) *Cort*$^{-/-}$ mice treated with saline solution or cortistatin at 24 h, to assess whether the treatment with the neuropeptide could impact the potential phenotype. Wild-type mice of the same age subjected to MCAO and injected with saline were used as controls (the data were incorporated in the graphs as a reference). Neurological score, behavioural performances, ischemic volume, glial population dynamics, BBB breakdown, and immune dynamics were analysed at 48 h. According to CV staining, young animals lacking cortistatin showed severe ischemic damage volumes (over 30 mm^3) when compared to *Cort*$^{+/+}$ animals (over 10 mm^3), although this trend was not significant, and were partially reduced after cortistatin treatment (Figure 1a,b). When MAP-2 staining was analysed, severe damage was found in *Cort*$^{-/-}$ mice compared to wild-type especially in the striatum. This feature was significantly reduced after

cortistatin treatment (Figure 1a,b). This enhanced neuronal damage in cortistatin-deficient mice was correlated with worse neurological scores (mean score 2-3, *i.e.,* motor incoordination, intermittent circling, and tremor twitches) compared to wild-type mice (mean score 1-1.5, *i.e.,* moderate hypomobility, moderate motor incoordination, intermittent circling), which were significantly decreased after cortistatin treatment (Figure 1c).

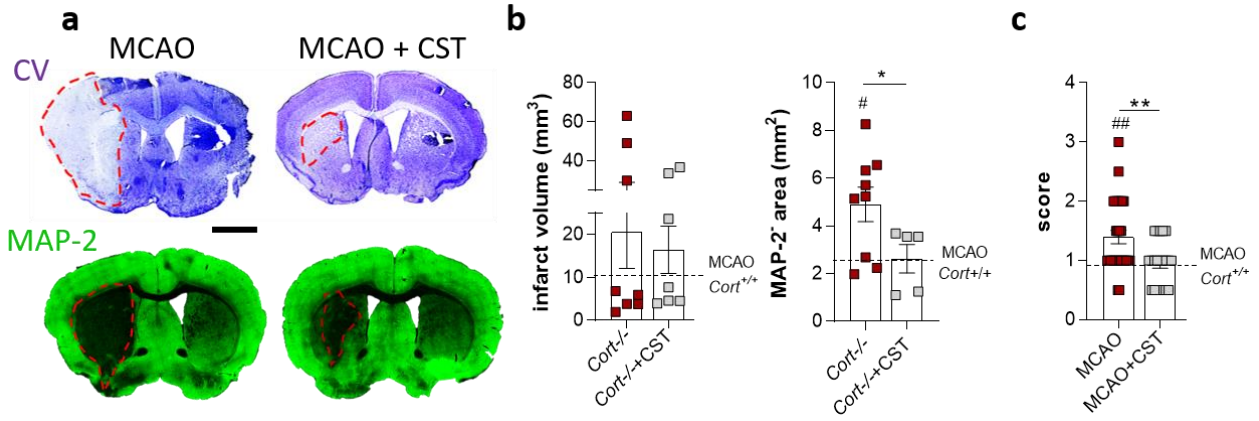

Figure 1. Cortistatin deficiency is associated with enhanced neuronal damage and worsened score, a condition that is reversed after cortistatin treatment. **a**. Brain coronal sections from *Cort*$^{-/-}$ mice subjected to MCAO and treated with either saline (MCAO) or cortistatin (144µg/kg) (MCAO+CST) at 24 h post-reperfusion and sacrificed at 48 h. Sections were stained with cresyl violet (CV) (up) or MAP-2 (down, green) to identify neuronal damage. Ischemic lesions are outlined with dashed red lines. Scale bar: 1,500µm. **b**. Ischemic volume across the brain was determined by measuring ten CV-stained brain slices at 2-mm intervals per mouse (left) or by quantifying the lack of MAP-2 staining in a coronal section (right). N = 5-9 mice/group. **c**. Neurological scores were assessed at 48h on a scale from 0 (no signs) to 3 (death). N = 6-13 mice/group. Mice were compared to *Cort*$^{+/+}$ MCAO saline-treated mice (dashed line). Data are expressed as mean ± SEM. **vs. Cort*$^{-/-}$ MCAO saline-treated mice, $^{\#}$*vs. Cort*$^{+/+}$ MCAO saline-treated mice, $^{*/\#}p \leq 0.05$, $^{**/\#\#}p \leq 0.01$. CST: cortistatin, MAP-2: microtubule-associated protein 2, MCAO: middle cerebral artery occlusion.

Given the severe neurological damage and exacerbated inflammatory responses generally observed in cortistatin-deficient mice [9], we further explored the neuroinflammatory response in these animals. Regarding microglia dynamics, we observed an increase in microglia density in the infarct core of *Cort*$^{-/-}$ mice compared to their contralateral side (Figure 2a), a density similar to that seen in *Cort*$^{+/+}$ mice. Cortistatin treatment did not affect microglia density in these animals (Figure 2a). Importantly, cortistatin-deficient microglia exhibited a distinct reactive morphotype compared to their homeostatic counterparts on the contralateral side (Figure 2b). In essence, these cells showed reduced number of junctions and branch length, reduced territory area, and increased soma (Figure 2c), compared to their contralateral cells. Notably, cortistatin treatment reversed all these features bringing them back to levels similar to those of the contralateral side, thereby reducing cell activation and promoting a more ramified-like phenotype (Figure 2b,c). Remarkably, although no differences were found in microglia density between wild-type and cortistatin-deficient mice, we noted that cortistatin-deficient cells displayed a reduced number of junctions when compared to their wild-type counterparts, suggesting a more reactive phenotype in the absence of cortistatin. Remarkably, there was a significant decrease in *CD163* expression after stroke in the ipsilateral brain hemisphere of

cortistatin-deficient animals compared with wild-type (Figure 2d), suggesting a potential reduction in the anti-inflammatory activity of these cells in the absence of cortistatin, consistent with the morphological findings (Figure 2b,c).

Complementary, we studied astrocytic dynamics. Surprisingly, cortistatin-deficient mice exhibited an impaired glial scar compared to wild-type controls, which was reversed by cortistatin treatment to baseline levels observed in MCAO wild-type mice (Figure 2e). Given this striking difference, we conducted a more detailed analysis of astrocyte morphology. Notably, after MCAO, astrocytes lacking cortistatin displayed an unusual phenotype characterized by smaller non-ramified elongated forms (Figure 2f). More specifically, they displayed shorter branch lengths, smaller soma, increased span ratios, and reduced territory coverage (Figure 2g) compared to wild-type astrocytes following MCAO. However, all of these aberrant parameters were reversed by the neuropeptide treatment (Figure 2f-g), leading to a more reactive and presumably functional phenotype (Figure 2f). To validate our findings, we examined the expression of GFAP, a well-known marker of astrocyte reactivity [24]. Following MCAO, cortistatin-deficient mice showed increased GFAP expression compared to the contralateral side and wild-type mice. No changes were observed after cortistatin treatment. Interestingly, the reduced expression of neurotrophic factors found after MCAO (similar to the one observed in wild-type mice) was increased after cortistatin treatment, especially for *Gdnf*.

In summary, these findings indicate that cortistatin deficiency is linked to a dysfunctional glial phenotype, which likely contributes to the observed exacerbated neuronal damage. However, cortistatin treatment appears to reverse this dysfunctional phenotype, promoting a more ramified state in microglia and a more reactive functional state in astrocytes, shift that seems crucial for mitigating neuronal damage in these animals.

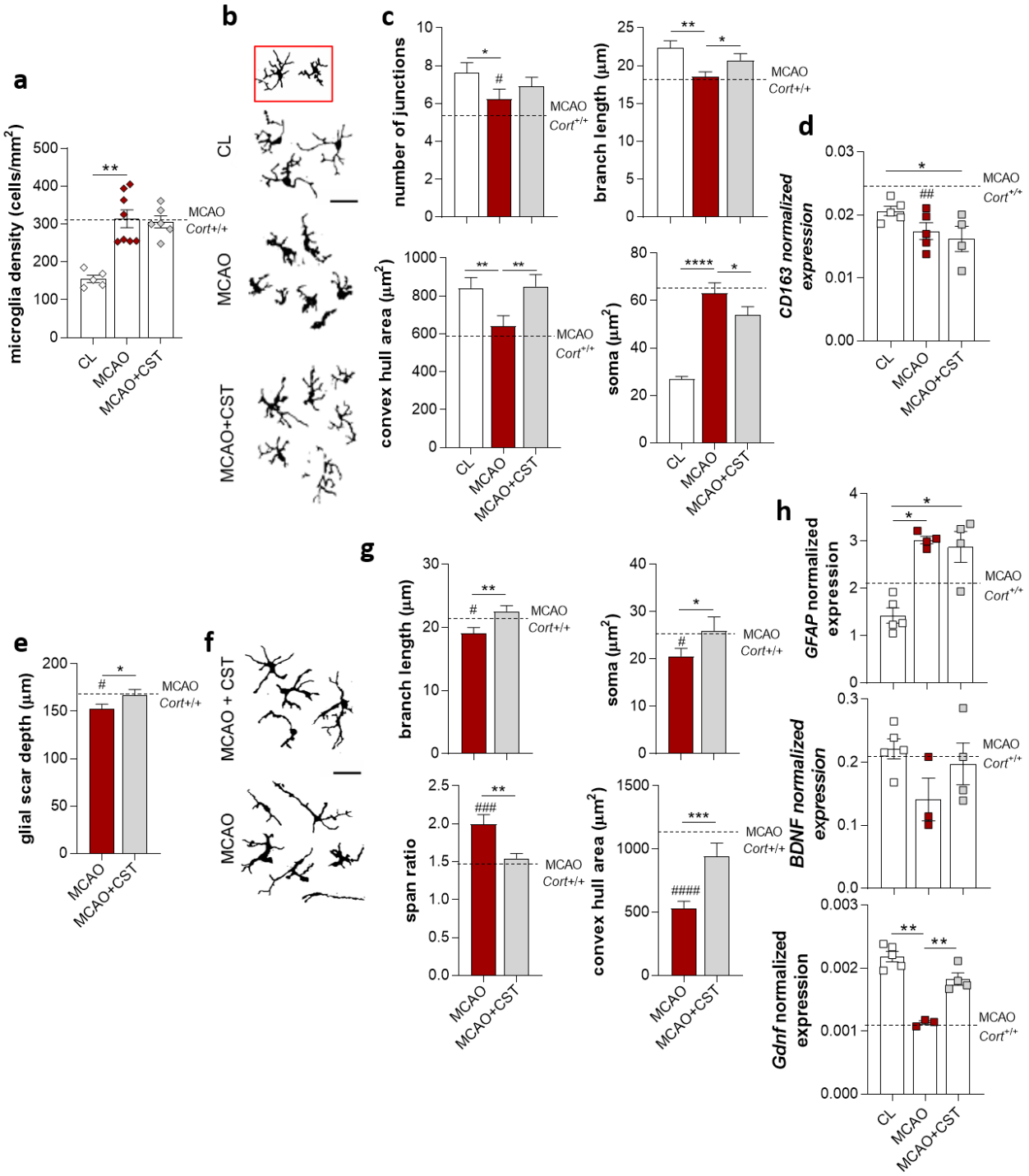

Figure 2. Deficiency of cortistatin is linked to exacerbated microglial response and impaired astrocytic scar which is modulated after cortistatin treatment. MCAO was conducted in *Cort*$^{-/-}$ mice treated with either saline (MCAO) or cortistatin (144µg/kg) (MCAO+CST) at 24 h post-reperfusion and sacrificed at 48 h. Mice were compared to *Cort*$^{+/+}$ MCAO saline-treated mice (dashed line). **a.** Density of microglia (cells/mm^2) was measured in the contralateral side/ischemic core in the above-mentioned mice. **b.** Representative binary microglia from the different experimental groups from the contralateral side or the penumbra. Scale bar: 30 µm. **c.** Morphological parameters analysed. Skeleton Analysis was used to assess the number of junctions and branch length (upper left and right panel). Cell territory (convex hull area) was analysed by Fractal Analysis (down left panel) and soma size (downright panel) was manually measured. n = 15-20 cells/mice; N = 3 mice/group. **d.** Gene expression levels of CD163 in the contralateral (CL, uninjured) and ipsilateral (ischemic) brain hemispheres of *Cort*$^{-/-}$ mice treated with saline or cortistatin following MCAO were analysed by real-time

qPCR and normalized to *Rplp0* expression. N = 4-5 mice/group. **e.** Glial scar thickness was quantified. N = 4-6 mice/group. **f.** Representative images of astrocytes in binary were extracted from the glial scar in the different experimental groups. Scale bar: 30 µm. **g.** Evaluation of morphological parameters of astrocytes. Branch length (upper left panel) was evaluated by Skeleton Analysis. Soma size (upper right panel) was manually measured. Span ratio (down left panel) and cell territory (convex hull area) (downright panel) were analysed by Fractal Analysis. n = 15-20 cells/mice; N = 3 mice/group. **h.** Gene expression levels of GFAP in the contralateral (CL, uninjured) and ipsilateral (ischemic) brain hemispheres of *Cort*$^{-/-}$ mice treated with saline or cortistatin following MCAO were analysed by real-time qPCR and normalized to *Rplp0* expression. N = 4-5 mice/group. Data represent the mean ± SEM. **vs. Cort*$^{-/-}$ MCAO saline-treated mice, $^{\#}$*vs. Cort*$^{+/+}$ MCAO saline-treated mice, $^{*/\#}p \leq 0.05$, $^{**/\#\#}p \leq 0.01$, $^{***/\#\#\#}p \leq 0.001$. CD163: cluster of differentiation 163, CST: cortistatin, GFAP: glial fibrillary acidic protein, MCAO: middle cerebral artery occlusion.

Cortistatin deficiency is associated with enhanced BBB breakdown, increased immune infiltration and severe immunodepression after stroke, which is reversed following cortistatin administration

Given the increased permeability observed in cortistatin-deficient mice following LPS inflammatory response, as well as the enhanced permeability of cortistatin-deficient endothelium under *in vitro* ischemic-like conditions in previous studies from our group [14], we examined BBB dynamics. First, we assessed IgG leakage (Figure 3a) and found an increased IgG leakage in MCAO *Cort*$^{-/-}$ mice compared to wild-type MCAO controls. However, cortistatin treatment significantly reduced the augmented leakage (Figure 3a). Furthermore, we investigated brain endothelium dynamics given the impaired peripheral endothelium already described for these mice [25]. While we observed that the vascular density was similar in cortistatin-deficient mice compared to wild-type mice after MCAO, there was a significant increase in the amount of vessels/area in mice lacking cortistatin after the treatment with the neuropeptide (Figure 3b). Regarding TJs disruption, although there was a similar number of gaps in ZO-1 structure compared to wild-type mice, cortistatin treatment significantly reduced the number of gaps (Figure 3c).

Finally, given the pro-inflammatory basal state of these animals [9], and the enhanced pro-inflammatory responses in other models [9,12], we investigated brain immune infiltration and peripheral immune responses. Importantly, there was a trend towards an enhanced CD45 infiltration in cortistatin-deficient mice after MCAO compared to wild-type but significantly modulated after cortistatin treatment (Figure 3d). Regarding brain cytokines levels after MCAO, as expected, *TNF-α* increased in the ipsilateral brain while *IL-10* expression decreased compared to their contralateral hemisphere (Figure 3e). Interestingly, cortistatin treatment enhanced both *TNF-α* and *IL-10* expression in *Cort*$^{-/-}$ MCAO mice. Notably, there was a trend to exacerbated *TNF-α* levels in *Cort*$^{-/-}$ mice compared to *Cort*$^{+/+}$ mice (Figure 3e). Additionally, we found a marked immunodepression in *Cort*$^{-/-}$ mice characterized by lymphopenia and decreased spleen weight compared to *Cort*$^{+/+}$ mice. However, cortistatin treatment reversed these effects, significantly increasing the total number of splenocytes and spleen weight after stroke (Figure 3f).

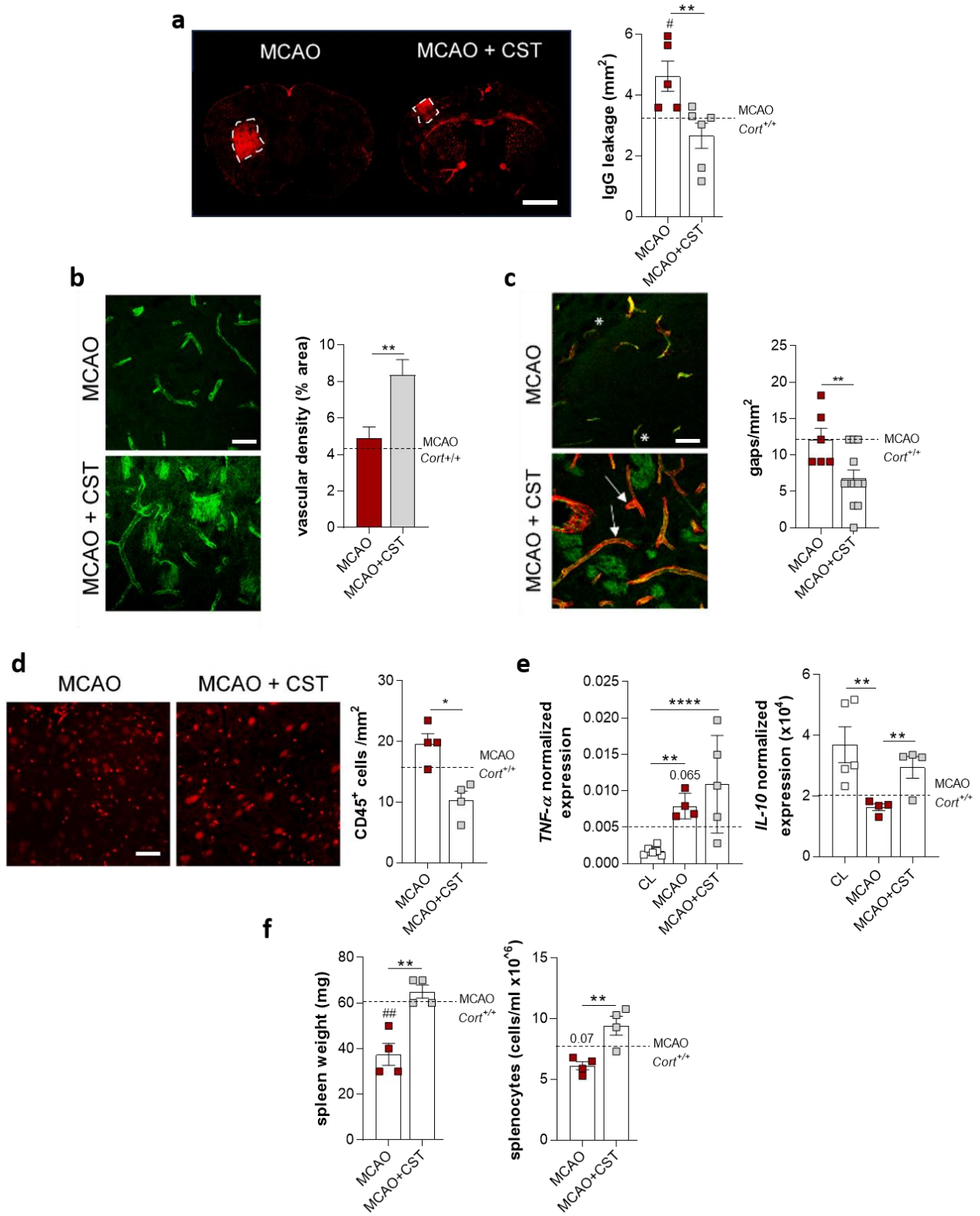

Figure 3. Absence of cortistatin leads to severe BBB breakdown, increased brain immune infiltration, and significant immunodepression after stroke, which is regulated following cortistatin administration. **a.** Brain coronal sections from *Cort*$^{-/-}$ mice treated with either saline (MCAO) or cortistatin (144µg/kg) (MCAO+CST) at 24 h post-reperfusion and sacrificed at 48 h. Sections were stained with a fluorescently-labelled antibody against mouse IgGs. IgG leakage areas are outlined with dashed white lines. Scale bar: 1,500 µm. IgG+ area (right) was measured as a quantification of IgG leakage from the blood. N = 4-6 mice/group. **b.** Left. Representative images taken in the ipsilateral striatum of *Cort*$^{-/-}$ mice following MCAO and treated with CST, stained with CD31 antibody for brain endothelial cells (BECs, green). Scale bar: 30 µm.

Right**.** Vascular density was calculated as the % of positive CD31 staining of the total area of the image. N = 3-6 mice/group. **c.** Left. Representative images taken in the ipsilateral striatum of *Cort*$^{-/-}$ mice following MCAO and treated with CST, stained with CD31 antibody for brain endothelial cells (BECs, green) and ZO-1 (red) for TJs. ZO-1 gaps are highlighted with an asterisk, while ZO-1 coverage recovery is indicated with arrows. Scale bar: 30 µm. Right. Quantification of the number of ZO-1 gaps per vessel area. n = 3 ROIs/section/mice; N = 6-12 mice/group. **d.** Left. Magnification of representative brain coronal sections stained with CD45 antibody (red) for leukocytes from the mentioned mice. Scale bar: 100 µm. Right. Leukocyte density (number of cells/mm^2) was measured in the striatum and the contralateral side (CL). **e**. Spleen weight and the number of splenocytes/ml were measured. N = 4 independent mice. **f**. Gene expression levels for *TNF-α* and *IL-10* in the contralateral and ipsilateral brain hemispheres of the mentioned mice were quantified using real-time qPCR and normalized to *Rplp0* expression. N = 4-6 independent mice. Mice were compared to *Cort*$^{+/+}$ MCAO saline-treated mice (dashed line). Data represent the mean ± SEM. **vs. Cort*$^{-/-}$ MCAO saline-treated mice, $^{\#}$*vs. Cort*$^{+/+}$ MCAO saline-treated mice, $^{*/\#}p \leq 0.05$, $^{**/\#\#}p \leq 0.01$, $^{****/\#\#\#\#}p \leq 0.0001$. CD31: cluster of differentiation 31, CD45: cluster of differentiation 45, CST: cortistatin, IgG: immunoglobulin G, MCAO: middle cerebral artery occlusion, IL-10: interleukin 10, TNF-α: tumour necrosis factor-α, ZO-1: zonula-occludens 1.

In summary, enhanced neuronal damage and dysfunctional glial response observed in MCAO *Cort*$^{-/-}$ mice are also associated with a disrupted BBB, leading to increased leakage and immune infiltration. Moreover, although there is an increase of pro-inflammatory factors and a decrease of anti-inflammatory mediators in the brain, a marked immunodepression occurs in the periphery compared to wild-type mice. The administration of exogenous cortistatin after stroke to mice lacking cortistatin, regulates BBB breakdown and local and peripheral immune responses.

Long-term treatment with cortistatin improves stroke outcomes, neuronal repopulation, axonal preservation, glial scar functionality and BBB breakdown protection

To further explore the endogenous and therapeutic roles of cortistatin at later stages (7 days post-stroke), we administered the neuropeptide for 7 days, starting 24 h after stroke, in young *Cort*$^{+/+}$ and *Cort*$^{-/-}$ mice. We observed a trend towards an increased infarct volume in *Cort*$^{-/-}$ mice at 7 days compared to wild-type mice. Similarly, there was a trend towards a reduction in infarct volume after cortistatin treatment, though the differences were not statistically significant (Figure 4a,b). However, cortistatin treatment in *Cort*$^{-/-}$ mice led to increased neuronal density (Figure 4b), indicating enhanced cell repopulation following the neuropeptide treatment. Similar trends were observed in MAP-2 staining (Figure 4c). Importantly, a reduced neurological deficit score was also observed after cortistatin treatment (Figure 4d) in both genotypes, supporting these findings. However, no differences were found between wild-type and cortistatin-deficient mice in terms of neurological score. However, after evaluating axonal damage with MBP, we found a greater area of disorganized and aberrant axonal structures in *Cort*$^{-/-}$ mice compared to wild-type mice. Administration of cortistatin reduced these myelin damage areas in both genotypes. The disrupted axonal organization was correlated with an increased mean grey value, suggesting compromised MBP folding, as previously described [26].

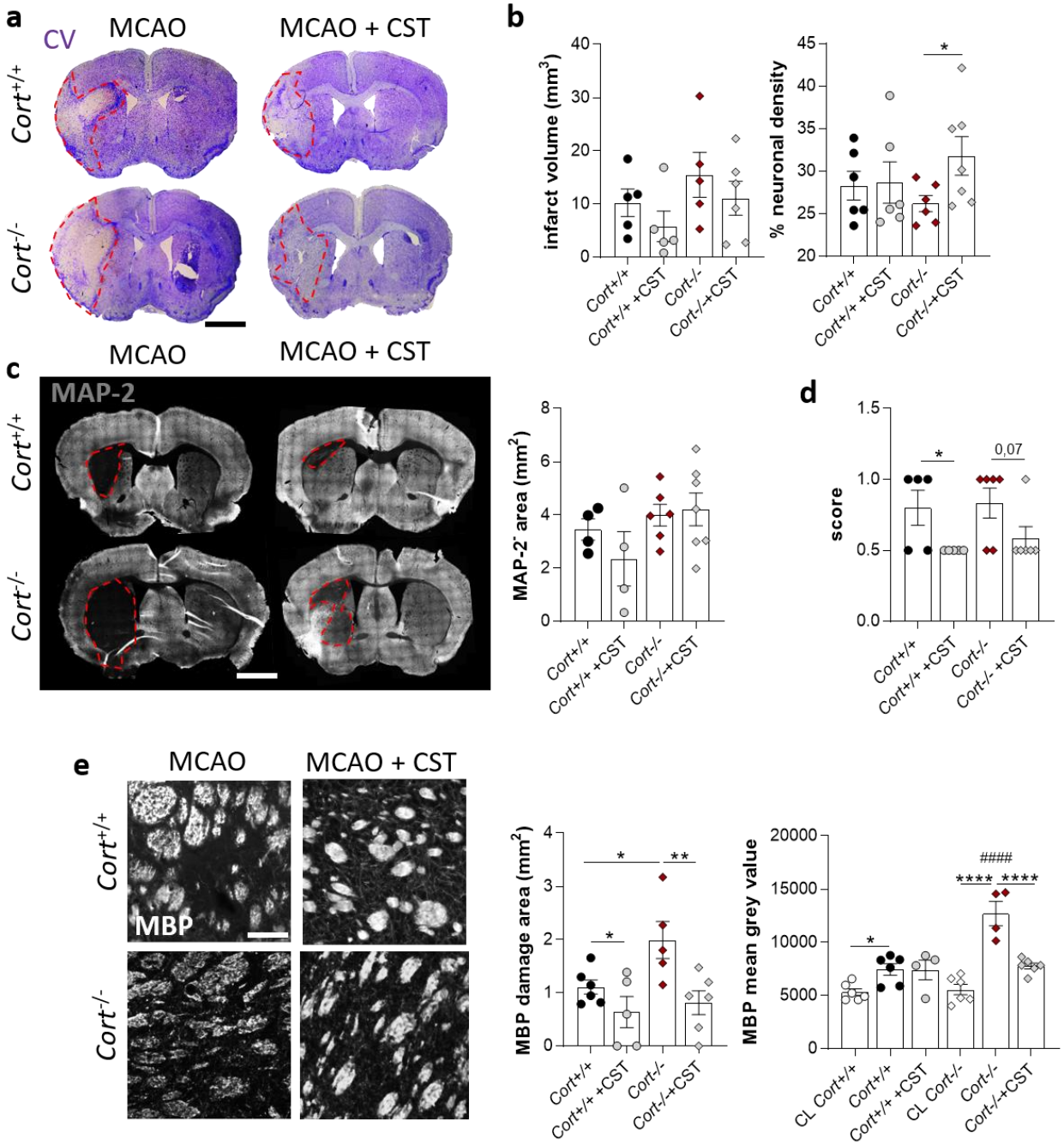

Figure 4. Long-term treatment with cortistatin is associated with improved stroke outcomes, neuronal repopulation, and axonal preservation. **a-c.** Brain coronal sections from *Cort*$^{+/+}$ and *Cort*$^{-/-}$ mice treated with either saline (MCAO) or cortistatin (144µg/kg) (MCAO+CST) each day starting 24 h post-reperfusion and sacrificed at 7 days. Sections were stained with cresyl violet (CV) (**a**) to identify neuronal damage. Ischemic lesions are outlined with dashed red lines. Scale bar: 1,500 µm. **b**. Left, ischemic volume across the brain was determined by measuring ten CV-stained brain slices at 2-mm intervals per mouse. Right, % of neural density in the ischemic area was quantified. **c.** Left. Sections were also stained with MAP-2 (green). Right**.** Lack of MAP-2 staining in a coronal section was analysed as a measure of neuronal damage. **d.** Neurological scores were assessed at 7th day on a scale from 0 (no signs) to 3 (death). N = 6-13 mice/group. **e.** Right. Representative images taken in the ipsilateral striatum of the mentioned mice stained with the MBP antibody for myelin sheaths. Scale bar: 30 µm. **f.** Area of damaged myelin sheaths was quantified (left) as well as the area of MBP mean grey value (right). N = 4-7 mice/group. Data represent the mean ± SEM. **vs.* MCAO cortistatin-treated mice, $^{\#}$*vs. Cort*$^{+/+}$ MCAO saline-treated mice, $^{*/\#}p \leq 0.05$, $^{**/\#\#}p \leq 0.01$, $^{****/\#\#\#\#}p \leq 0.0001$. CST: cortistatin, MAP-2: microtubule-associated protein 2, MBP: myelin basic protein, MCAO: middle cerebral artery occlusion.

We then examined glial dynamics and BBB disruption at these later stages. Notably, while there were no differences in microglia density within genotypes and treatments (Figure 5a,b), we observed an increased glial scar thickness in *Cort*$^{-/-}$ mice compared to wild-type mice (Figure 5c,d), contrasting with our findings at 48 h (Fig 2e). Cortistatin treatment reduced scar thickness in both genotypes, suggesting that the glial scar in cortistatin-deficient mice may transition from non-functional at 48 h to becoming fibrotic and excessive at later stages. This highlights that a key role of cortistatin is to regulate the proper development of the scar at each stage.

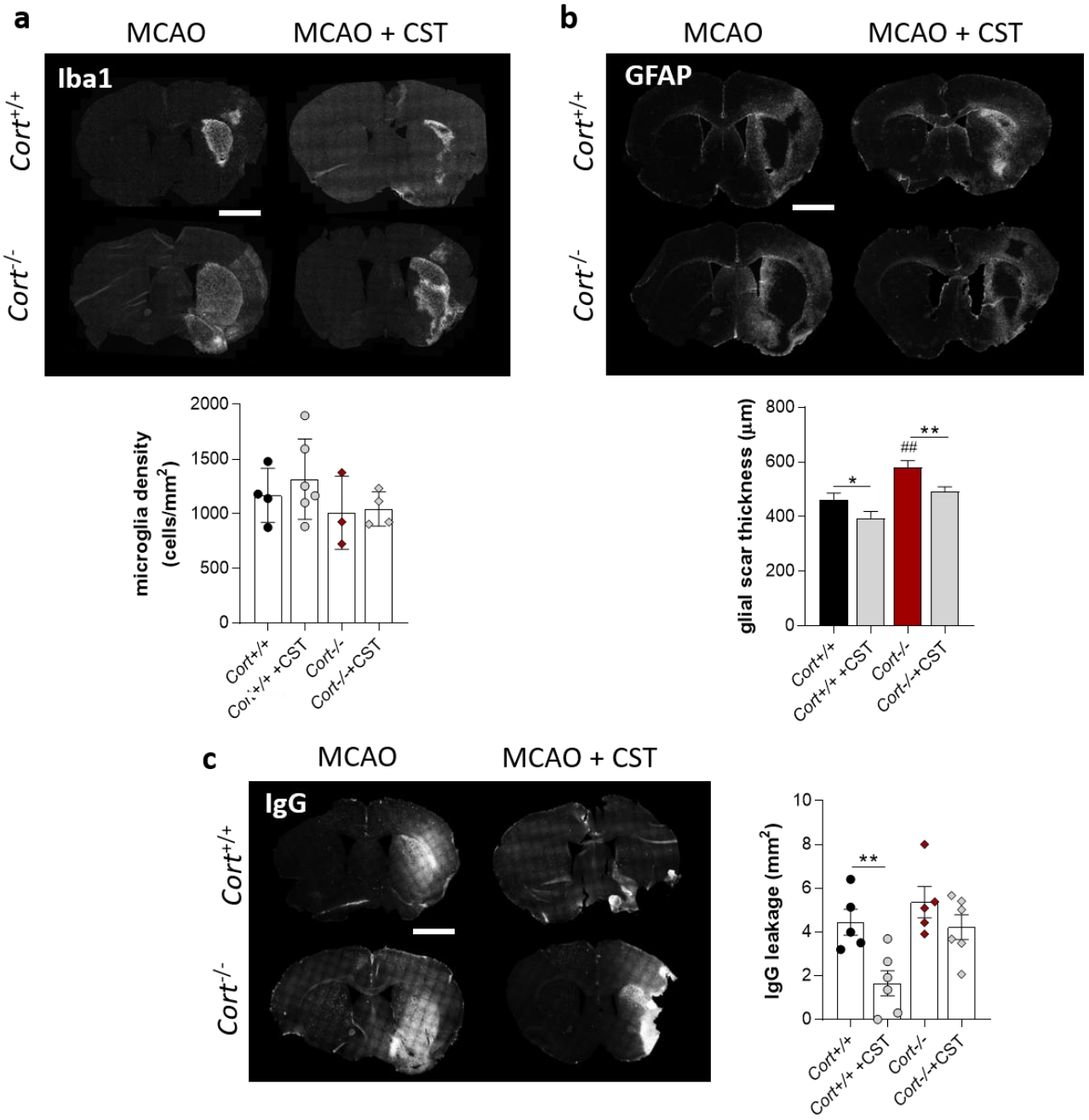

Figure 5. Cortistatin deficiency at 7 days post-stroke is linked to excessive glial scar, which is reversed by cortistatin treatment. Brain coronal sections from *Cort*$^{+/+}$ and *Cort*$^{-/-}$ mice treated with either saline (MCAO) or cortistatin (144µg/kg) (MCAO+CST) each day starting 24 h post-reperfusion and sacrificed at 7 days. **a.** Up. Representative sections stained with Iba1 to identify microglia. Down. Density of microglia (cells/mm^2) was measured in the contralateral side/ischemic core in the above-mentioned mice. **b.** Up. GFAP antibody was used to identify astrocytes. Scale bar: 1,500µm. Down. Glial scar thickness was quantified. N = 4-6 mice/group.

c. Up. Sections were stained with a fluorescently-labelled antibody against mouse IgGs. Scale bar: 1,500 µm. Down. IgG+ area was measured as a quantification of IgG leakage from the blood. N = 4-8 mice/group. Data represent the mean ± SEM. **vs.* MCAO cortistatin-treated mice, $^{\#}$*vs. Cort*$^{+/+}$ MCAO saline-treated mice, $^{*/\#}p \leq 0.05$, $^{**/\#/\#}p \leq 0.01$. CST: cortistatin, Iba1: ionized calcium-binding adaptor molecule 1, IgG: immunoglobulin G, GFAP: glial fibrillary acidic protein, MCAO: middle cerebral artery occlusion.

Regarding BBB dynamics, we found a trend towards increased disruption in *Cort*$^{-/-}$ mice compared to wild-type mice. However, cortistatin treatment significantly reduced this leakage, aligning with our observations at 48 h (Figure 5c).

In summary, we found that after 7 days, stroke severity in cortistatin-deficient mice particularly manifests in glial scar formation, neuronal repopulation, and axonal integrity, key processes essential for neuronal recovery and neurogenesis at this stage, and different from those at 48 h. Importantly, the administration of exogenous cortistatin after stroke was able to reverse most pathological features in both genotypes, suggesting that its pleiotropic neuroprotective effects can extend beyond the 48-hour mark to promote long-term recovery.

Cortistatin-deficient middle-aged mice display hyper-ramified microglia, impaired glial scar, enhanced BBB leakage and increased immune infiltration after stroke, which is reversed following cortistatin administration

Next, after examined the endogenous role of cortistatin in short and long-term outcomes, as well as its potential therapeutic role, we aimed to further investigate its functions introducing an important stroke risk factor (aging). For this, we conducted the model in and middle-aged (6 months old) *Cort*$^{+/+}$ and *Cort*$^{-/-}$ mice. Mice were treated with saline solution or cortistatin at 24 h, to assess whether the treatment could impact the potential phenotype. Data from young (3 months old) mice injected with saline were used as a reference (dashed line in the graphs). As described above, neurological score, behavioural performances, ischemic volume, glial population dynamics, BBB breakdown, and immune dynamics were analysed at 48 h.

We first sought to investigate the ischemic lesion volume through the evaluation of CV and MAP-2 in these mice. Surprisingly, we did not observe larger lesions with this methodology in older *Cort*$^{-/-}$ mice (Figure 6a). However, ischemic damage assessed by MAP-2 was more extensive in middle-aged *Cort*$^{+/+}$ mice compared to young mice (Figure 6b). Importantly, there was a reduction after cortistatin treatment in middle-aged wild-type mice. Interestingly, middle-aged animals of both genotypes exhibit a similar score to young mice, although there was a significant severe score in middle-aged mice compared to wild-type animals. Additionally, there was a trend towards an improved score after cortistatin treatment (Figure 6c).

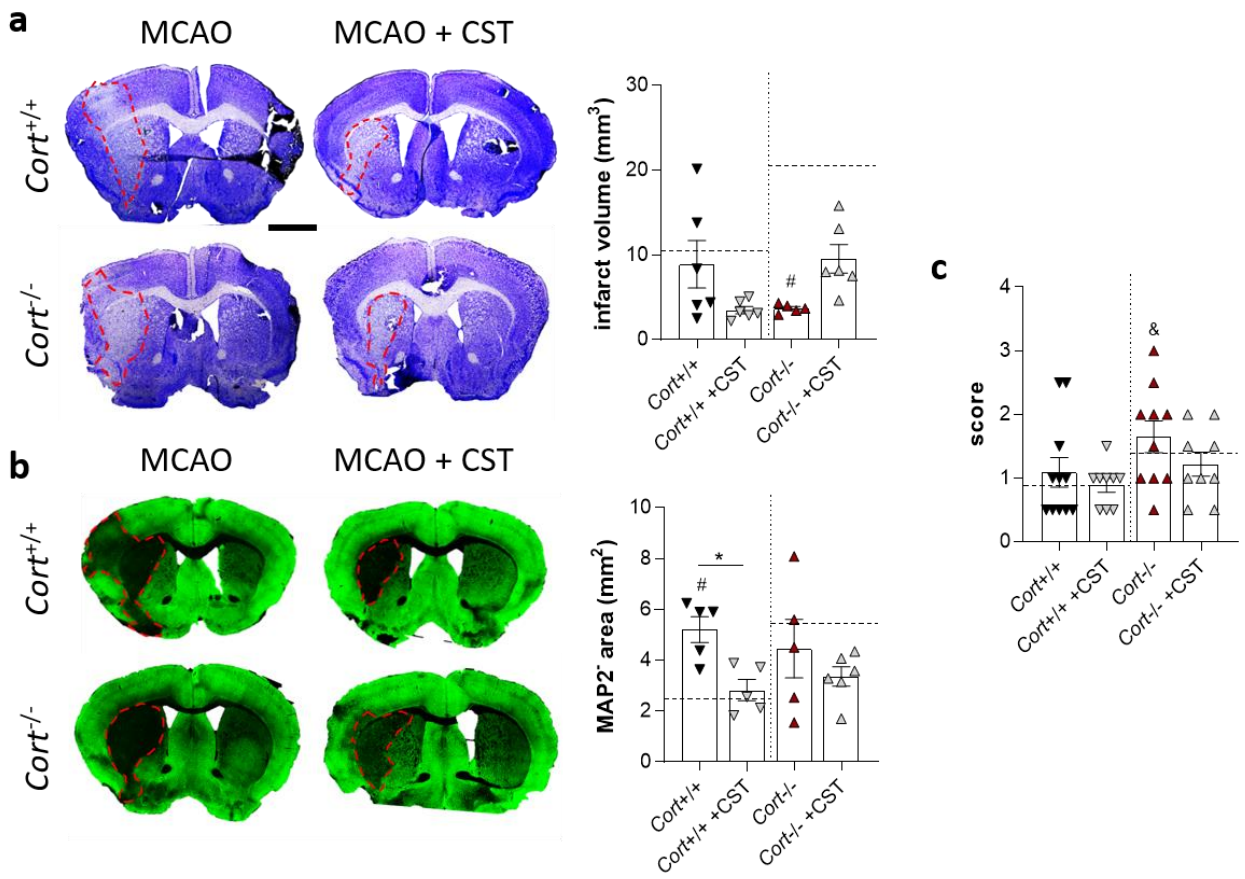

Figure 6. a-b. Cortistatin-deficient middle-aged mice exhibit similar neurological damages to young and wild-type mice. Brain coronal sections from 6-month-old *Cort*$^{+/+}$ and *Cort*$^{-/-}$ mice subjected to MCAO and treated with either saline (MCAO) or cortistatin (144µg/kg) (MCAO+CST) at 24 h post-reperfusion and sacrificed at 48 h. Sections were stained with cresyl violet (CV) (**a**) or MAP-2 (**b**, green) to identify neuronal damage. Ischemic lesions are outlined with dashed red lines. Scale bar: 1,500µm. Ischemic volume across the brain was determined by measuring ten CV-stained brain slices at 2-mm intervals per mouse (**a**, right) or by quantifying the lack of MAP-2 staining in a coronal section (**b**, right). Mice were compared to young *Cort*$^{+/+}$ and *Cort*$^{-/-}$ MCAO saline-treated mice (dashed line). N = 5-6 mice/group. **c.** Neurological scores were assessed at 48h on a scale from 0 (no signs) to 3 (death). N = 9-12 mice/group. Data are expressed as mean ± SEM. **vs. Cort*$^{+/+}$ or *Cort*$^{-/-}$ MCAO cortistatin-treated mice, $^{\#}$*vs.* young *Cort*$^{+/+}$ or *Cort*$^{-/-}$ MCAO saline-treated mice, $^{\&}$*vs.* middle-aged *Cort*$^{+/+}$ MCAO saline-treated mice $^{*/\#}p \leq 0.05$. CST: cortistatin, MAP-2: microtubule-associated protein 2, MCAO: middle cerebral artery occlusion.

Regarding glial dynamics, we observed enhanced microglia density in cortistatin-deficient mice compared to the contralateral side (Figure 7a), similar to what we observed in young mice (Figure 2a). Upon careful evaluation of microglia morphotypes, we noted that *Cort*$^{+/+}$ middle-aged microglia showed larger soma, reduced branch length, and smaller territory compared to their contralateral microglia, highlighting their reactive morphotype. Importantly, cortistatin reversed most of these features to a more ramified-like state (Figure 7b-e). Remarkably, *Cort*$^{-/-}$ middle-aged microglia exhibited increased soma, fewer junctions, and increased territory regarding their contralateral microglia. Although these parameters and the phenotype indicate a clearly reactive phenotype, it is important to highlight the differences compared to wild-type cells (*i.e.,* reduced number of junctions, increased branch length and territory) which points to a distinct hyper-ramified phenotype in

cortistatin-deficient cells (Figure 7b-e). Interestingly, middle-aged wild-type microglia also showed a more pronounced reactive morphotype when compared to young mice (*i.e.,* reduced soma, increased number of junctions, reduced branch length). Similarly, the hyper-ramified morphotype exhibited by middle-aged cortistatin-deficient microglia was markedly different from that of young cortistatin-deficient microglia (Figure 7b-e).

Interestingly, cortistatin-deficient astrocytes displayed an unusual phenotype characterized by small, non-ramified, elongated forms. Specifically, these astrocytes exhibited fewer junctions, shorter branch lengths, reduced territory coverage, and decreased complexity compared to wild-type astrocytes following MCAO (Figure 7g-j). These parameters were very similar to those observed in young mice (Figure 3f), except for an even more reduced number of junctions likely associated with age-related susceptibility. However, most of these aberrant parameters were reversed by neuropeptide treatment (Figure 7g-j), with astrocytes transitioning to a more reactive and presumably functional phenotype. Interestingly, we found that wild-type middle-aged astrocytes exhibited a phenotype similar to that of young astrocytes, with the exception of an increased number of junctions, complexity, and span ratio. especially in the older ones (Figure 7g-j).

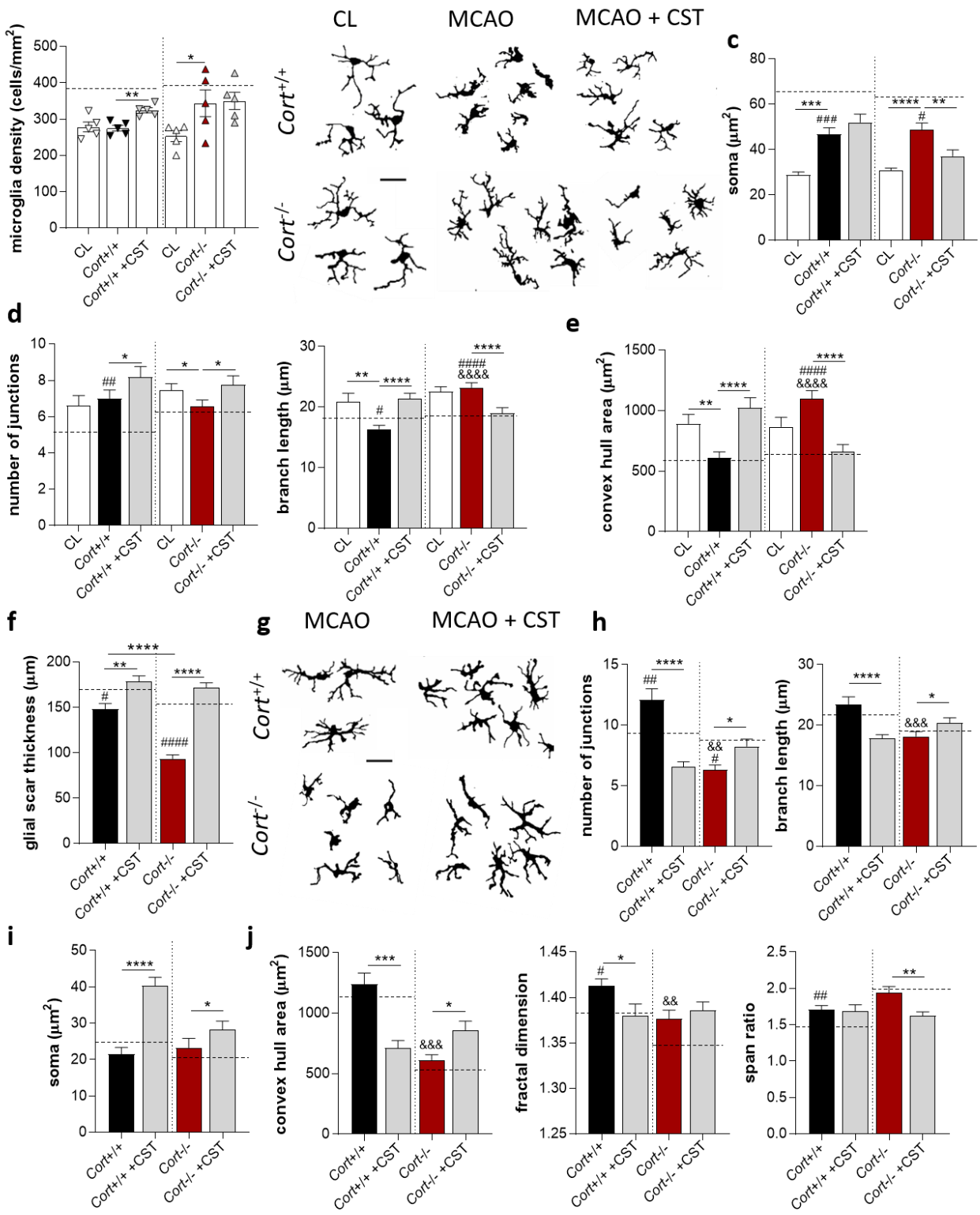

Figure 7. Cortistatin-deficient middle-aged mice exhibit hyper-ramified microglia and astrocytic impaired response. 6-month-old *Cort*$^{+/+}$ and *Cort*$^{-/-}$ mice were subjected to MCAO and treated with either saline (MCAO) or cortistatin (144µg/kg) (MCAO+CST) at 24 hours post-reperfusion and sacrificed at 48 hours. **a.** Density of microglia (cells/mm^2) was measured in the contralateral side/ischemic core in the above-mentioned mice. **b**. Representative binary microglia from the different experimental groups from the contralateral side (CL) or the penumbra. Scale bar: 30µm. **c-e.** Morphological parameters analysed. Soma size (**c**) was manually measured. Skeleton Analysis was used to assess the number of junctions and branch length (**d**). Cell territory (convex hull area) was analysed by Fractal Analysis (**e**). n = 15-20 cells/mice; N = 3

mice/group. **f.** Analysis of glial scar thickness. **g.** Representative images of astrocytes in binary were extracted from the glial scar in the different experimental groups. Scale bar: 30µm. **h-j.** Evaluation of morphological parameters of astrocytes. Number of junctions and branch length (**h**) was evaluated by Skeleton Analysis. Soma size (**i**) was manually measured. Cell territory (convex hull area) (**j**, left), fractal dimension (**j,** centre), and span ratio **(j**, right) was analysed by Fractal Analysis. n = 15-20 cells/mice; N = 3 mice/group. Mice were compared to young *Cort*$^{+/+}$ and *Cort*$^{-/-}$ MCAO saline-treated mice (dashed line). Data represent the mean ± SEM. **vs.* MCAO saline-treated mice, $^{\#}$*vs.* young *Cort*$^{+/+}$ / *Cort*$^{-/-}$ MCAO saline-treated mice, $^{\&}$*vs. Cort*$^{+/+}$ MCAO saline-treated mice, $^{*/\#/\&}p \leq 0.05$, $^{**/\#\#/\&\&}p \leq 0.01$, $^{***/\#\#\#/\&\&\&}p \leq 0.001$, $^{****/\#\#\#\#/\&\&\&\&}p \leq 0.0001$. CST: cortistatin, MCAO: middle cerebral artery occlusion.

After investigating the role of cortistatin in glial dynamics in post-ischemic stroke and given the lack of knowledge on cortistatin role in middle-aged mice, we examine BBB dynamics in these animals after stroke. For this, we conducted an analysis of IgG leakage (Figure 8a). In this case, we found increased IgG leakage in *Cort*$^{-/-}$ mice compared to wild-type controls (Figure 8a). However, cortistatin treatment significantly reduced the augmented leakage in this age group, as it did in young mice (Figure 4a). No differences were found between young and middle-aged mice in any of the genotypes. Importantly, this enhanced leakage was linked to reduced vascular density and diameter in cortistatin-deficient middle-aged mice compared to the younger ones. However, cortistatin treatment, as it did in young mice (Figure 4b), enhanced vascular density in both genotypes (Figure 8b). Regarding TJs disruption, no differences were found in ZO-1 disruption between young and middle-aged mice or between genotypes, but we observed a reduction in the number of ZO-1 gaps after cortistatin treatment in middle-aged wild-type mice, as it did in young animals (Figure 8c). Remarkably, this exacerbated leakage was associated with increased immune infiltration in both genotypes compared to young mice, a condition that was efficiently reversed following cortistatin treatment. Notably, cortistatin-deficient mice exhibited greater immune infiltration than both wild-type mice and their younger counterparts (Figure 8d).

In summary, MCAO *Cort*$^{-/-}$ middle-aged mice displayed dysfunctional microglia and astrocyte response, disrupted BBB, and enhanced immune infiltration than their younger counterparts. Remarkably, the beneficial effect of cortistatin administration on stroke outcomes affects both young and middle-aged animals.

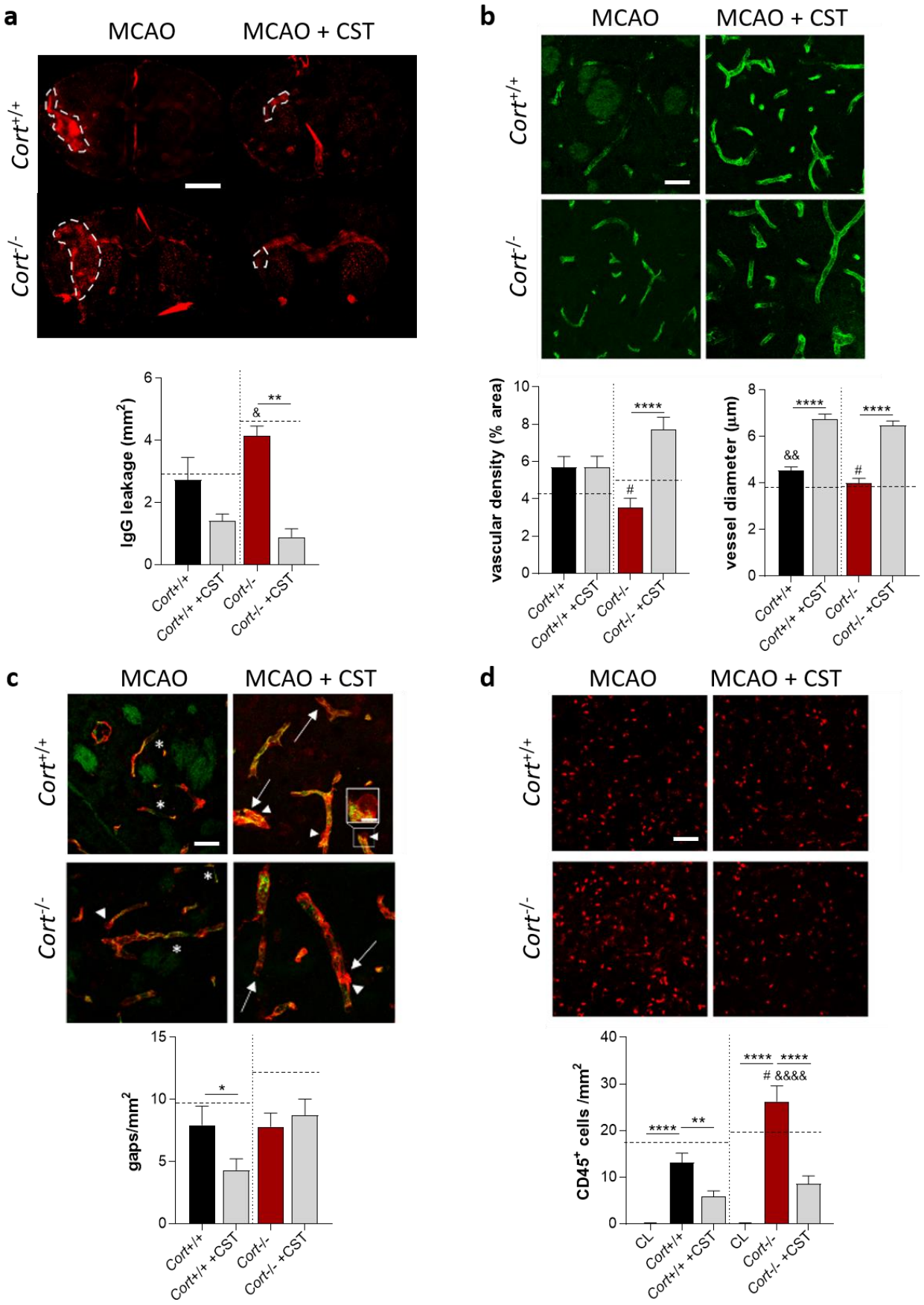

Figure 8. Cortistatin deficiency in middle-aged mice is linked to BBB leakage and severe immune infiltration. 6-month-old *Cort*$^{+/+}$ and *Cort*$^{-/-}$ mice were subjected to MCAO and treated with either saline

(MCAO) or cortistatin (144µg/kg) (MCAO+CST) at 24 hours post-reperfusion and sacrificed at 48 hours. **a.** Up. Representative sections stained with a fluorescently-labelled antibody against mouse IgGs. Down. IgG leakage areas are outlined with dashed white lines. Scale bar: 1,500 µm. IgG+ area was measured as a quantification of IgG leakage from the blood. N = 4-6 mice/group. **b.** Up. Representative images taken in the ipsilateral striatum of the mentioned mice stained with CD31 antibody for brain endothelial cells (BECs, green). Scale bar: 30 µm. Down. Vascular density was calculated as the % of positive CD31 staining of the total area of the image (down left) and vessel diameter was calculated manually (down right). N = 3-6 mice/group. **c.** Up. Representative images from the ipsilateral striatum of the mentioned mice, stained with CD31 antibody for brain endothelial cells (BECs, green) and ZO-1 (red) for TJs. ZO-1 gaps are highlighted with an asterisk, while ZO-1 coverage recovery is indicated with arrows. Scale bar: 30 µm. Down. Quantification of the number of ZO-1 gaps per vessel area. n = 3 ROIs/section/mice; N = 3-5 mice/group. **d.** Up. Representative magnifications of brain striatum stained with CD45 antibody (red) for leukocytes from the mentioned mice. Scale bar: 100µm. Down. Leukocyte density (number of cells/mm^2) was measured in the striatum and the contralateral side (CL). Data represent the mean ± SEM. **vs.* MCAO cortistatin-treated mice, $^{\#}$*vs. Cort*$^{+/+}$ MCAO saline-treated mice, $^{\&}$*vs. Cort*$^{+/+}$ / *Cort*$^{-/-}$ young mice, $^{*/\#/\&}p \leq 0.05$, $^{**/\#\#/\&\&}p \leq 0.01$, $^{****/\#\#\#\#/\&\&\&\&}p \leq 0.0001$. CD31: cluster of differentiation 31, CD45: cluster of differentiation 45, CST: cortistatin, IgG: immunoglobulin G, MCAO: middle cerebral artery occlusion, ZO-1: zonula-occludens 1.

DISCUSSION

The pathogenesis of stroke is a highly intricate process in which various types of nervous, circulating, and cerebral immune cells exert profound dual roles depending on their cell context, spatial location, and timing [4]. The complexity of this pathophysiology presents a significant challenge in designing therapeutic approaches, contributing to stroke remaining the second leading cause of death worldwide. Therefore, gaining a deeper understanding of the intricate relationship between the nervous, vascular, and immune systems and the endogenous mediators participating, is essential for improving stroke prognosis. To this aim, we explored for the first time the endogenous role of this neuropeptide in a preclinical model of stroke (MCAO), and examined whether the therapeutic role of cortistatin might reverse the phenotype.

The major immediate consequence of acute stroke is irreversible neuronal cell death and brain damage [27]. Interestingly, despite exhibiting poorer neurological deficits, we did not observe more severe lesions in cortistatin-deficient animals compared to wild-type. In this line, our results conform to other studies reporting that infarct size does not always correlate with neurological function and functional outcomes [289,290,305]. This suggests that the evaluation of stroke outcomes does not only have to rely on ischemic volumes. Importantly, we did find a reduction in the lesion size observed in the striatum with MAP-2 staining, which indicates that cortistatin targets these initial critical stages of neuronal death and it is especially important protecting neuronal bodies. However, the precise mechanisms underlying the influence of cortistatin in neurological lesions are not fully understood (*i.e.,* whether it directly inhibits apoptosis, neuronal degeneration, oxidative damage, or a combination of these factors). Accordingly, the questions of whether cortistatin exerts a direct neuroprotective effect on neurons or if, conversely, it is exerting other responses (*i.e.,* anti-inflammatory, immunomodulatory effects) on different cells, indirectly benefiting neurons, stand and remain a possibility that cannot be discarded.

In the first hours following ischemic stroke, microglia rapidly respond and accumulate in the infarct core and the peri-infarct zone [28]. Our observations revealed an enhanced number of microglia in the ischemic core in cortistatin-deficient mice, suggesting their potential involvement in the phagocytosis of dead neurons. However, whether the phagocytic function of microglia in stroke is advantageous or detrimental remains uncertain, highlighting the importance of maintaining a delicate balance for improved stroke prognosis. Given the enhanced neuronal damage observed in these mice, along with the reduction of anti-inflammatory factors such as CD163, and the more reactive phenotype of microglia in the penumbra compared to wild-type mice, our results suggest that these microglia may be hyper-reactive, potentially engulfing live or stressed neuronal cells and resulting in worsened neurological deficits, as previously reported by others [29]. Notably, previous studies from our group have demonstrated that while wild-type microglia produce neurotrophic and regenerative mediators and efficiently eliminate debris, cortistatin-deficient microglia exhibit deficient phagocytosis in both physiological and demyelinating environments [26].

Beyond microglia, astrocytes greatly contribute to the neuroinflammatory response. After ischemic damage astrocytes proliferate and migrate, creating a barrier around the edges of severely damaged tissue from the surrounding viable neural tissue [30]. Notably, the molecular and cellular mechanisms that underlie the formation of the glial scar and astrocyte reactivity are not completely understood. These likely involve a complex and balanced interplay of molecular signals that can simultaneously boost phagocytosis and debris clearance, which would be essential for the protection and conservation of the still-healthy tissue [30–32]. In this research, we described an impaired glial scar formation in cortistatin-deficient mice in both age groups. Interestingly, although very scarce, these astrocytes display a completely different phenotype from wild-type mice after stroke, exhibiting small, non-ramified, elongated forms, not previously described in the bibliography. Interestingly, these results did not align with previous descriptions from astrocytes in cortistatin-deficient mice in other neuroinflammatory models, such as EAE [9] or Parkinson's [13]. In detail, these studies showed no impaired response of astrocytes in cortistatin-deficient mice, rather, an upregulated astrogliosis was observed, which was reversed by cortistatin treatment. However, it is interesting to note that in these models, damage was evaluated at chronic stages, where the astrocyte response might be chronic and detrimental. Therefore, the most beneficial response in stroke at this stage would be to enhance the astrocytic response, as the underlying astrocytes would likely adopt a protective phenotype towards neurons. Accordingly, defective astrocyte scar formation in various transgenic loss-of-function models of ischemia has been shown to result in increased lesion size, demyelination, and death of local neurons, leading to decreased recovery of function [31–34].

On the other hand, BBB breakdown stands out as a primary hallmark of stroke, manifesting shortly after artery occlusion and persisting for several days to weeks [35]. However, BBB permeability exhibits a multiphasic pattern across various stroke stages (*i.e.,* hyperacute, acute, subacute, and chronic stages), each associated with distinct biological events [36]. Notably, our findings revealed an increased IgG leakage after stroke in cortistatin-deficient animals. This

observation is consistent with the increased BBB leakage previously reported by our group in a model of mild neuroinflammation induced by bacterial LPS, that also courses with BBB disruption [14]. Interestingly, cortistatin-deficient mice exhibited BBB disruption even under physiological conditions, confirming the great susceptibility of the barrier of these animals. Remarkably, the treatment with cortistatin mitigated this increased leakage, and could therefore be an important therapeutic advantage for this severe complication [14]. The disruption of the BBB is generally linked to endothelial damage and disrupted TJs and AJs. In this sense, we focused our study on the endogenous and therapeutic role of cortistatin in endothelial dynamics after ischemic injury and reperfusion. We found that cortistatin-deficient mice exhibited more gaps in ZO-1 structure after MCAO, when compared to their wild-type counterparts. Notably, cortistatin treatment could reduce this enhanced number of gaps This aligns with previous results where we demonstrated that BECs isolated from cortistatin-deficient mice exhibited both a disrupted BBB endothelium in homeostatic conditions, exacerbated after ischemic damage (*i.e.,* enhanced permeability, TJ-AJs disruption, increased pro-inflammatory state). Importantly, the exogenous addition of cortistatin reversed all these features [14].

Finally, it is important to recognize that a stroke is a complex process affecting not only the brain but also peripheral tissues throughout the body. Following the interruption of blood flow and subsequent hypoxia, endothelial cells quickly respond to oxidative damage by expressing selectins, which active circulating innate immune cells, and trigger a peripheral pro-inflammatory response. This, combined with the breakdown of the BBB, facilitates the infiltration of immune cells [4]. Our investigation shows that cortistatin modulates immune infiltration in the brain of cortistatin-deficient mice. Similar effects were found by our group in an EAE model [9] and in a BBB *in vitro* model, where we observed that cortistatin can modulate the transmigration of macrophages and T cells across the endothelium [14]. To what extent cortistatin is involved in regulating adhesion molecules, whether is directly affecting immune cells instead, or both, are subjects that we cannot fully elucidate at this point. In fact, cortistatin exerts immunomodulatory activities in activated macrophages *in vitro,* suggesting that we cannot dismiss the latter [37]. As highlighted when addressing the neuroinflammatory response, we again advocate that understanding each specific mechanism at each specific stage seems to be paramount to achieving a better modulation of the overall response.

Beyond periphery-only effects, the elevation of inflammatory mediators following ischemia occurs both centrally and peripherally [38]. In general, an increased production of pro-inflammatory cytokines and a decreased production of anti-inflammatory cytokines are correlated with poorer clinical outcomes and larger infarct size in animal models [39]. In this sense, we observed enhanced levels of TNF-α and reduced levels of IL-10 in cortistatin-deficient mice. Moreover, these factors were significantly modulated after cortistatin treatment in both age groups, underlining the endogenous role of cortistatin as a mediator/brake in excessive inflammation, together with its potent anti-inflammatory properties when used as therapy.

Finally, it is important to bear in mind that stroke predominantly affects the elderly, with aging not merely being a risk factor but also linked to increased vulnerability and diminished capacity to recover from brain injury [40]. Despite this, most studies are currently conducted in young animals, leaving the impact of aging relatively unexplored. Typically, older animals (15-24 months old) are employed to study the aging component in stroke [41,42]. However, cortistatin-deficient mice already manifest an elevated susceptibility to various injury models [9,12,43,44], as well as a premature aging-like phenotype that is evident as early as 6 months (unpublished data). Consequently, the use of older animals might have compromised the success of the model due to the probable high mortality of these animals. Moreover, it is important to note that the incidence rates in people under the age of 70 have worryingly risen in the last 20 years, accounting for 63% of strokes [45]. Therefore, studies conducted in middle-aged are also of great relevance.

Notably, we do not find differences in neuronal damage between young and middle-aged animals in any of the genotypes. Despite this being surprising, several studies in rodents and humans have reported that aging is not necessarily correlated to developing a larger infarct size, even if aged individuals recover less effectively than younger ones [41,42]. For instance, Gullota and collaborators reported worsened neurological outcomes and higher mortality rates, but without increased neuronal lesions [46,47]. This may be attributed to the fact that, although the timing of neuronal loss in aged rats is accelerated, the process of neuronal degeneration ultimately converges on a similar endpoint in young and old individuals [46]. This would explain the lack of differences between young and middle-aged mice, both in wild-type or cortistatin-deficient mice. Hence, we advocate that the reductions in ischemic lesions by cortistatin in both age groups and genotypes are of particular interest and value.

Similarly, our findings showed that cortistatin treatment at later stages reduced lesion sizes, but did not show a significant improvement in the neurological score of wild-type mice. These non-significant differences in score, despite an evident reduction in the neuronal lesion, may be attributed to the use of a mild rather than a severe stroke model. Indeed, in the mild model, clinical manifestations are very similar between low scores, making it challenging to observe the correlation between infarct volume and scores [48]. Nevertheless, mild models also induce less damage and reduced endothelial lining injury [49]. Importantly, cortistatin-deficient mice exhibited worsened neurological scores in both age groups compared to wild-type mice. Accordingly, higher susceptibility of cortistatin-deficient mice has been observed in other injury models [50–53]. Importantly, cortistatin treatment reduced neurological scores in cortistatin-deficient young and middle-aged mice. The capacity of cortistatin to regulate neurological deficits in older mice or those more susceptible to stroke, which present severe clinical manifestations (*i.e.,* cortistatin-deficient mice), is highly promising.

Nevertheless, we did find differences in the neuroinflammatory response, since clearly hyper-ramified microglia was observed in middle-aged *Cort*$^{-/-}$ mice compared to wild-type and

their respective young mice. Interestingly, other studies have reported hyper-ramification of microglia in response to acute and chronic stress and excitotoxicity, a response that might be implicated in synaptic modifications [51,54]. For instance, Hinwood and colleagues reported that chronic stress resulted in hyper-ramified microglia in the prefrontal cortex of rats, correlating with enhanced activation of neurons in that region and impaired spatial working memory [55]. This is in line with the stress-like behaviour exhibited by these animals and may imply an hyperreactivity of these cells prior to ischemia which may negatively impact the posterior neurological damage. Accordingly, other studies from our group indicated exacerbated inflammatory responses in cortistatin-deficient microglia [9]. Importantly, cortistatin treatment modulated this phenotype, resembling microglia found in MCAO wild-type mice in some properties while mirroring the microglia observed in healthy wild-type animals in most of the parameters.

Furthermore, we found that cortistatin-deficient endothelium in middle-aged mice exhibited a greater number of infiltrated immune cells in the brain parenchyma following injury. Similarly, in previous studies, we observed enhanced migration of macrophages and T cells through the cortistatin-deficient brain endothelium [14]. Although the precise underlying mechanisms are not fully understood, it is possible that endogenous cortistatin regulates the adhesion and transmigration of these cells across the endothelium. However, we cannot rule out the role of the disrupted endothelium in these mice in promoting leukocyte migration, nor the contribution of inflammatory factors or chemokines from other cells within the brain parenchyma.

Therefore, although not many changes were found between wild-type young and middle-aged mice, there were dramatic alterations regarding microglia activity, astrocytic scar formation, BBB disruption, and immune infiltration between cortistatin-deficient wild-type young and middle-aged. This confirms that cortistatin is a key endogenous factor that modulates in a multifactorial way stroke pathogenesis, and its deficiency, combined with the risk factor of aging, provokes significant changes that may affect the long-term progression of the disorder. Importantly, cortistatin treatment modulated many of these features in cortistatin-deficient young and middle-aged mice. The capacity of cortistatin to regulate neurological deficits in older mice or those more susceptible to stroke which present severe clinical manifestations (*i.e.,* cortistatin-deficient mice), is highly promising. This suggests that this neuropeptide could also effectively target challenging stroke manifestations.

Since MCAO represents an acute cerebrovascular event, and given the treatment windows for tPA (4-6 hours) and endovascular therapies (up to 24 hours), studying endogenous mechanisms and therapeutic tools within the first 48 hours is critical. This period is crucial for neuronal damage, glial reactivity, BBB breakdown, and immune modulation, with early events largely dictating long-term outcomes. After addressing the endogenous and potential therapeutic role of cortistatin in the acute phase, we aimed to study its role in the long-term.

Remarkably, we found that after 7 days, stroke severity in cortistatin-deficient mice manifests differently than at 48 hours. At 48 hours, cortistatin deficiency is characterized by increased neuronal damage, impaired neurological scores, dysfunctional glial activity, and BBB breakdown, key factors influencing early responses. However, by 7 days, cortistatin plays a crucial role in glial scar formation, neuronal repopulation, and axonal integrity, processes essential for neuronal recovery and neurogenesis at this stage. Notably, the administration of exogenous cortistatin after stroke reversed most pathological features in both genotypes, suggesting that its pleiotropic neuroprotective effects extend beyond the 48-hour window, promoting long-term recovery. These results underscore the importance of cortistatin at each stage of the ischemic pathology. It is also important to note that the role of cortistatin differs within the same structure at each stage. For instance, in cortistatin-deficient mice, we observed an impaired glial scar at 48 hours, a critical time when scar formation is necessary to prevent damage from spreading to viable areas. However, by 7 days, these same mice exhibited excessive glial scarring, which can be harmful, as it may exacerbate inflammation or interfere with synapse sprouting and axon growth during the recovery phase.

In conclusion, cortistatin stands as a pleiotropic endogenous key factor and a potential therapeutic agent in stroke management. In particular, its role in modulating several pathological features, such as clinical manifestations, neurological damage, glial over-reaction, astrocyte scar, or BBB breakdown holds significant promise compared to interventions targeting only a single aspect. Furthermore, cortistatin emerges as a critical factor modulating the intricate interplay between the CNS and the immune system, regulating exacerbated cellular and molecular responses from both systems that could impact brain homeostasis. Finally, its efficient application at short and long-term outcomes and across different ages and phenotypes could open the door for extending a therapeutic time window, which is unfortunately very narrow or non-existent for many patients who do not meet the clinical criteria. The useful insights derived from this study have the potential to contribute to the development of novel therapeutic strategies not only for stroke, but also for other CNS pathologies associated with BBB dysfunction, glial over-reactivity, or impaired CNS-immune system interplay.

ACKNOWLEDGEMENTS

The authors would like to thank the Animal Care Unit and Microscopy Service Unit staff from IPBLN for the technical support.

FUNDING

This work was supported by the Spanish Ministry of Economy and Competitiveness (MCIN)/Spanish Research Agency (AEI)/10.13039/501100011033 grants: SAF2017-85602-R (to E.G-R.), FPU-program FPU17/02616 (to J.C-G.), FPI-program PRE2018-084824 (to I.S-M.) and PRE2021-100172 (to P.V-R.), the Swiss Science Foundation FNS 310030_212233 grant to L.H, and the European Molecular Biology Organization EMBO-STFL8942 grant to J.C-G.

CONTRIBUTIONS

EG-R conceived, designed and supervised the whole study. J.C-G and E.G-R outlined the experiments and analysed all the data. J.C-G, P.V-R, I.S-M, and I.F-L performed the experiments. J.C-G, L.B, M.P, P.H-C, L.H, and .EG-R interpreted the data, and discussed the results. J.C-G and E.G-R wrote and revised the manuscript. All authors have read and agreed to the published version of the manuscript.

BIBLIOGRAPHY

1. Campbell BCV, De Silva DA, Macleod MR, Coutts SB, Schwamm LH, Davis SM, et al. Ischaemic stroke. Nat Rev Dis Primers. 2019;5:1–22.

2. Iadecola C, Anrather J. The immunology of stroke: from mechanisms to translation. Nat Med. 2011;17:796–808.

3. Drieu A, Levard D, Vivien D, Rubio M. Anti-inflammatory treatments for stroke: from bench to bedside. Ther Adv Neurol Disord. 2018;11:1756286418789854.

4. Anrather J, Iadecola C. Inflammation and Stroke: An Overview. Neurotherapeutics. 2016;13:661–70.

5. de Lecea L, Criado JR, Prospero-Garcia O, Gautvik KM, Schweitzer P, Danielson PE, et al. A cortical neuropeptide with neuronal depressant and sleep-modulating properties. Nature. 1996;381:242–5.

6. Delgado M, Gonzalez-Rey E. Role of Cortistatin in the Stressed Immune System. In: Savino W, Guaraldi F, editors. Frontiers of Hormone Research. S. Karger AG; 2017. p. 110–20

7. Córdoba-Chacón J, Gahete MD, Pozo-Salas AI, Martínez-Fuentes AJ, de Lecea L, Gracia-Navarro F, et al. Cortistatin is not a somatostatin analogue but stimulates prolactin release and inhibits GH and ACTH in a gender-dependent fashion: potential role of ghrelin. Endocrinology. 2011;152:4800–12.

8. Deghenghi R, Papotti M, Ghigo E, Muccioli G. Cortistatin, but not somatostatin, binds to growth hormone secretagogue (GHS) receptors of human pituitary gland. J Endocrinol Invest. 2001;24:RC1-3.

9. Souza-Moreira L, Morell M, Delgado-Maroto V, Pedreño M, Martinez-Escudero L, Caro M, et al. Paradoxical Effect of Cortistatin Treatment and Its Deficiency on Experimental Autoimmune Encephalomyelitis. J Immunol. 2013;191:2144–54.

10. Braun H, Schulz S, Becker A, Schröder H, Höllt V. Protective effects of cortistatin (CST-14) against kainate-induced neurotoxicity in rat brain. Brain Res. 1998;803:54–60.

11. Chiu C-T, Wen L-L, Pao H-P, Wang J-Y. Cortistatin Is Induced in Brain Tissue and Exerts Neuroprotection in a Rat Model of Bacterial Meningoencephalitis. J Infect Dis. 2011;204:1563–72.

12. Falo CP, Benitez R, Caro M, Morell M, Forte-Lago I, Hernandez-Cortes P, et al. The Neuropeptide Cortistatin Alleviates Neuropathic Pain in Experimental Models of Peripheral Nerve Injury. Pharmaceutics. 2021;13:947.

13. Serrano-Martínez I, Pedreño M, Castillo-González J, Ferraz-de-Paula V, Vargas-Rodríguez P, Forte-Lago I, et al. Cortistatin as a novel multimodal therapy for the treatment of Parkinson´s Disease. Int J Mol Sci. 2023;5;25(2):694

14. Castillo-González J, Ruiz JL, Serrano-Martínez I, Forte-Lago I, Ubago-Rodriguez A, Caro M, et al. Cortistatin deficiency reveals a dysfunctional brain endothelium with impaired gene pathways, exacerbated immune activation, and disrupted barrier integrity. J Neuroinflammation. 2023;20:226.

15. Castillo-González J, Buscemi L, Vargas-Rodríguez P, Serrano-Martínez I, Forte-Lago I, Price M, et al. Cortistatin exerts an immunomodulatory and neuroprotective role in a preclinical model of ischemic stroke. bioRxiv. doi.org/10.1101/2024.02.07.579281

16. Barriga M, Benitez R, Robledo G, Caro M, O'Valle F, Campos-Salinas J, et al. Neuropeptide Cortistatin Regulates Dermal and Pulmonary Fibrosis in an Experimental Model of Systemic Sclerosis. Neuroendocrinology. 2021;112:784–95.

17. Buscemi L, Price M, Bezzi P, Hirt L. Spatio-temporal overview of neuroinflammation in an experimental mouse stroke model. Sci Rep. 2019;9:507.

18. Lee H. Disruption of the blood-brain barrier in parkinson's disease: curse or route to a cure? Front Biosci. 2014;19:272.

19. Buscemi L, Price M, Castillo-González J, Chatton J-Y, Hirt L. Lactate Neuroprotection against Transient Ischemic Brain Injury in Mice Appears Independent of HCAR1 Activation. Metabolites. 2022;12:465.

20. Young K, Morrison H. Quantifying Microglia Morphology from Photomicrographs of Immunohistochemistry Prepared Tissue Using ImageJ. JoVE. 2018;57648.

21. Fernández-Arjona M del M, Grondona JM, Granados-Durán P, Fernández-Llebrez P, López-Ávalos MD. Microglia Morphological Categorization in a Rat Model of Neuroinflammation by Hierarchical Cluster and Principal Components Analysis. Front Cell Neurosci. 2017;11:235.

22. Schindelin J, Arganda-Carreras I, Frise E, Kaynig V, Longair M, Pietzsch T, et al. Fiji: an open-source platform for biological-image analysis. Nat Methods. 2012;9:676–82.

23. Wang J, Zhang P, Tang Z. Animal models of transient ischemic attack: a review. Acta Neurol Belg. 2020;120:267–75.

24. Jurga AM, Paleczna M, Kadluczka J, Kuter KZ. Beyond the GFAP-Astrocyte Protein Markers in the Brain. Biomolecules. 2021;11:1361.

25. Duran-Prado M, Morell M, Delgado-Maroto V, Castaño JP, Aneiros-Fernandez J, de Lecea L, et al. Cortistatin Inhibits Migration and Proliferation of Human Vascular Smooth Muscle Cells and Decreases Neointimal Formation on Carotid Artery Ligation. Circ Res. 2013;112:1444–55.

26. Pérez Falo C. Papel del neuropéptido cortistatina en la fisiopatología de los procesos de des- y remielinización en el sistema nervioso [Internet] [http://purl.org/dc/dcmitype/Text]. Universidad de Granada; 2021 [cited 2023 Nov 27]. p. 1. Available from: https://dialnet.unirioja.es/servlet/tesis?codigo=295627

27. Fan C, Zhang L, He Z, Shao P, Ding L, Wang G, et al. Reduced Severity of Outcome of Recurrent Ipsilateral Transient Cerebral Ischemia Compared with Contralateral Transient Cerebral Ischemia in Rats. J Stroke Cerebrovasc Dis. 2017;26:2915–25.

28. Peng L, Hu G, Yao Q, Wu J, He Z, Law BY-K, et al. Microglia autophagy in ischemic stroke: A double-edged sword. Front Immunol. 2022;13.

29. Neher JJ, Emmrich JV, Fricker M, Mander PK, Théry C, Brown GC. Phagocytosis executes delayed neuronal death after focal brain ischemia. Proc Natl Acad Sci U S A. 2013;110:E4098–107.

30. Shen X-Y, Gao Z-K, Han Y, Yuan M, Guo Y-S, Bi X. Activation and Role of Astrocytes in Ischemic Stroke. Front Cell Neurosci. 2021;15:755955

31. Burda JE, Sofroniew MV. Reactive Gliosis and the Multicellular Response to CNS Damage and Disease. Neuron. 2014;81:229–48.

32. Wanner IB, Anderson MA, Song B, Levine J, Fernandez A, Gray-Thompson Z, et al. Glial Scar Borders Are Formed by Newly Proliferated, Elongated Astrocytes That Interact to Corral Inflammatory and Fibrotic Cells via STAT3-Dependent Mechanisms after Spinal Cord Injury. J Neurosci. 2013;33:12870–86.

33. Faulkner JR, Herrmann JE, Woo MJ, Tansey KE, Doan NB, Sofroniew MV. Reactive astrocytes protect tissue and preserve function after spinal cord injury. J Neurosci. 2004;24:2143–55.

34. Herrmann JE, Imura T, Song B, Qi J, Ao Y, Nguyen TK, et al. STAT3 is a critical regulator of astrogliosis and scar formation after spinal cord injury. J Neurosci. 2008;28:7231–43.

35. Bernardo-Castro S, Sousa JA, Brás A, Cecília C, Rodrigues B, Almendra L, et al. Pathophysiology of Blood–Brain Barrier Permeability Throughout the Different Stages of Ischemic Stroke and Its Implication on Hemorrhagic Transformation and Recovery. Front Neurol. 2020;11:594672

36. Castillo-González J, Gonzalez-Rey E. Beyond wrecking a wall: Revisiting the concept of blood-brain barrier breakdown in ischemic stroke. Neural Regen Res. 2024;2.

37. Gonzalez-Rey E, Chorny A, Robledo G, Delgado M. Cortistatin, a new antiinflammatory peptide with therapeutic effect on lethal endotoxemia. J Exp Med. 2006;203:563–71.

38. Saunders NR, Dziegielewska KM, Møllgård K, Habgood MD. Markers for blood-brain barrier integrity: how appropriate is Evans blue in the twenty-first century and what are the alternatives? Front Neurosci. 2014;8:404

39. Doll DN, Barr TL, Simpkins JW. Cytokines: Their Role in Stroke and Potential Use as Biomarkers and Therapeutic Targets. Aging Dis. 2014;5:294–306.

40. Yousufuddin M, Young N. Aging and ischemic stroke. Aging (Albany NY). 2019;11:2542–4.

41. Ritzel RM, Lai Y-J, Crapser JD, Patel AR, Schrecengost A, Grenier JM, et al. Aging alters the immunological response to ischemic stroke. Acta Neuropathol. 2018;136:89–110.

42. Sieber MW, Claus RA, Witte OW, Frahm C. Attenuated Inflammatory Response in Aged Mice Brains following Stroke. PLoS One. 2011;6:e26288.

43. Benitez R, Caro M, Andres-Leon E, O'Valle F, Delgado M. Cortistatin regulates fibrosis and myofibroblast activation in experimental hepatotoxic- and cholestatic-induced liver injury. Br J Pharmacol. 2022;179:2275–96.

44. Barriga M, Benitez R, Ferraz-de-Paula V, Garcia-Frutos M, Caro M, Robledo G, et al. Protective role of cortistatin in pulmonary inflammation and fibrosis. Br J Pharmacol. 2021;178:4368–88.

45. Feigin VL, Stark BA, Johnson CO, Roth GA, Bisignano C, Abady GG, et al. Global, regional, and national burden of stroke and its risk factors, 1990–2019: a systematic analysis for the Global Burden of Disease Study 2019. The Lancet Neurology. 2021;20:795–820.

46. Popa-Wagner A, Carmichael ST, Kokaia Z, Kessler C, Walker L. The Response of the Aged Brain to Stroke: Too Much, Too Soon? Curr Neurovasc Res. 2007;4:216–27.

47. Gullotta GS, De Feo D, Friebel E, Semerano A, Scotti GM, Bergamaschi A, et al. Age-induced alterations of granulopoiesis generate atypical neutrophils that aggravate stroke pathology. Nat Immunol. 2023;24:925–40.

48. Benakis C, Garcia-Bonilla L, Iadecola C, Anrather J. The role of microglia and myeloid immune cells in acute cerebral ischemia. Front Cell Neurosci. 2015;8:461

49. Qin C, Zhou L-Q, Ma X-T, Hu Z-W, Yang S, Chen M, et al. Dual Functions of Microglia in Ischemic Stroke. Neurosci Bull. 2019;35:921–33.

50. Stuckey SM, Ong LK, Collins-Praino LE, Turner RJ. Neuroinflammation as a Key Driver of Secondary Neurodegeneration Following Stroke? Int J Mol Sci. 2021;22:13101.

51. Vidal-Itriago A, Radford RAW, Aramideh JA, Maurel C, Scherer NM, Don EK, et al. Microglia morphophysiological diversity and its implications for the CNS. Front Immunol. 2022;13:997786

52. Herpich F, Rincon F. Management of Acute Ischemic Stroke. Critical Care Medicine. 2020;48:1654.

53. Cai W, Liu H, Zhao J, Chen LY, Chen J, Lu Z, et al. Pericytes in Brain Injury and Repair After Ischemic Stroke. Transl Stroke Res. 2017;8:107–21.

54. Choi YH, Laaker C, Hsu M, Cismaru P, Sandor M, Fabry Z. Molecular Mechanisms of Neuroimmune Crosstalk in the Pathogenesis of Stroke. Int J Mol Sci. 2021;22:9486.

55. Hinwood M, Morandini J, Day TA, Walker FR. Evidence that Microglia Mediate the Neurobiological Effects of Chronic Psychological Stress on the Medial Prefrontal Cortex. Cerebral Cortex. 2012;22:1442–54.